

OPTIMIZATION OF A DIFFUSER GEOMETRY USING PARAMETRIC MODELING TOOLS AND FINITE-DIFFERENCE TIME-DOMAIN SIMULATIONS

J Meyer Dept. of Computer Science, Aalto University, Helsinki, Finland
T Lokki Dept. of Computer Science, Aalto University, Helsinki, Finland

1 INTRODUCTION

The inclusion of diffusing surfaces in an enclosed space is of primary importance in the spatial distribution of the reflected sound waves it produces. It is therefore of interest to evaluate the directional uniformity of the surface scattering and try to find geometries that would create the most uniform scattered polar distribution around it. There exist numerous studies on the optimization of such diffusing surfaces using various modeling techniques (boundary element method (BEM), finite-difference time-domain method (FDTD)) and several optimization algorithms (downhill simple algorithm, genetic algorithms)^{1,2}. This paper presents an approach for optimizing a diffuser geometry using parametric modeling tools and finite-difference time-domain (FDTD) acoustic simulations as well as a Bayesian optimization algorithm. Such an approach can be used to facilitate and speed up the design process of diffusers that can provide a good trade-off between performance and relatively simple geometry. Cox and d'Antonio³ mention that three key ingredients are necessary to optimize the shape of a diffuser:

- A validated prediction model. Here, the FDTD method is chosen.
- A figure of merit or error parameter. Here, the single-valued broadband diffusion parameter is used.
- An optimization algorithm to change the diffuser geometry. Here, a Bayesian approach is employed.

This paper is organized as follows. First, the candidate geometries tested in the optimization process are described. Second, the procedure to extract the scattered polar responses predicted using room acoustic FDTD simulations is explained. The simulation results are then analyzed in terms of the uniformity of the scattering produced by the diffusing surface and expressed in a single figure of merit that is used as the fitness value in the optimization process. In a third part, the optimization algorithm working principle is briefly presented and the results from the optimization process are presented in a fourth section before conclusions. The overview of the full optimization process is illustrated in Figure 1 below.

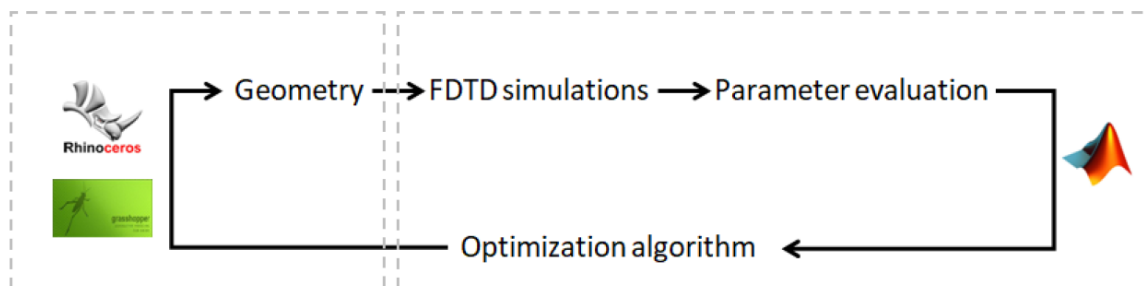


Figure 1: Overview of the optimization process.

2 GEOMETRY

An existing diffuser prototype with rectangular bars oriented diagonally was first chosen as a starting point of the optimization process. However, in order to limit the computational demands (memory and GPU requirements) and the numerical dispersion associated with FDTD simulations, the grid space resolution was set to 3 cm. Since the first proposed diffuser prototype did not match with this constraint, a new diffuser geometry based on the diffuser prototype was designed to serve as the starting point of the optimization process. As for the first proposed diffuser prototype, the new diffuser geometry consists in a single pattern duplicated 8 times undergoing a rotation of either 0°, 90° or 180° from its area centroid, and distributed across the diffuser surface. The pattern, the resulting 3D model of the diffuser that was optimized and the 3D mesh used in the numerical simulations are shown in Figure 2. Within this pattern, two geometrical parameters were chosen to vary for being optimized, namely the depth and the width of the bars. The depth of the bars was set to vary within three possibilities (5 cm, 10 cm or 15 cm) for all of the bars together whereas each of the five bars could vary with two different widths (either 3 cm or 4 cm), resulting in a total of $3 \times 2^5 = 96$ candidate geometries. Each of these candidates was exported in the form of a list of vertex coordinates (in meters), and a list of triangle indices defining the geometry. To allow for automatic generation of these geometries, a plug-in using the Rhinoceros 3D computer-aided design (CAD) software together with its integrated visual programming language and environment Grasshopper was developed. The whole parametric space constituted of the 96 candidate geometries was first entirely evaluated in order to validate the use of the optimization algorithm.

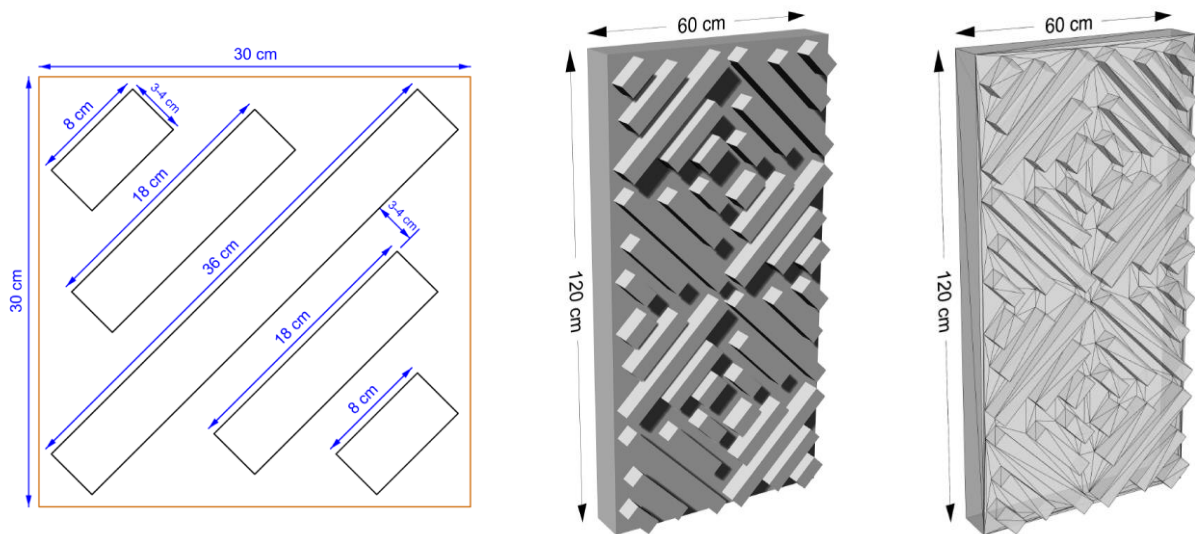


Figure 2: Front view of the pattern varying (left), 3D model of the resulting diffuser geometry (center), and 3D model of the mesh used in the simulations (right).

3 FDTD SIMULATIONS AND PARAMETER EVALUATION

3.1 Measurement setup

In order to describe the directional uniformity of the scattering that corresponds to the diffusing quality of the surface, the diffusion coefficient is measured. Two recently published standards focused on methods to measure the degree of diffusion created by surfaces^{4,5}. In the present paper, the method described in the ISO 17497-2 standard to measure the directional diffusion coefficient of surfaces in a free field has been followed. The measurement setup to measure the diffusion coefficient, illustrated in Figure 3, consists in placing receivers at 5 m and sources at 10 m on a semicircle around the test surface, measured from its center. To limit the computational cost of the numerical simulations employed to measure the directional uniformity of the scattering, the maximal source and receiver

resolution angles recommended in the ISO standard were chosen (10° and 5°, respectively), thus resulting in a number of $19 \times 37 = 703$ impulse responses to compute and evaluate for each of the 96 geometries.

In this paper, the diffusing quality of the geometries is calculated from the scattered polar responses predictions using the standard rectilinear (SRL) scheme of the FDTD method⁶. Because of the non-fully absorbent nature of the room boundary surfaces in the FDTD method, a rectangular box of dimensions (32.5 x 45 x 25) m was designed to make sure that no reflections from the test surface overlaps with the reflection from the room boundary surfaces in the impulse response. Although this results in a big domain and therefore long impulse responses to compute, it is useful for the spectral resolution of the resulting impulse response, especially in the low frequency region. In the simulations, a hard source with a delta function as the driving excitation function was used to irradiate the test surface. A sampling frequency of 20 kHz was used so that the simulation results were valid up to a cutoff frequency of 2000 Hz with a ~2% dispersion error⁷. For each source, the computational time was of approximately one hour. Simulations were run simultaneously on three different computers using three GPUs each for maximizing the speed of the process, thus resulting in a total of ~25 days for computing all the 96 candidate geometries.

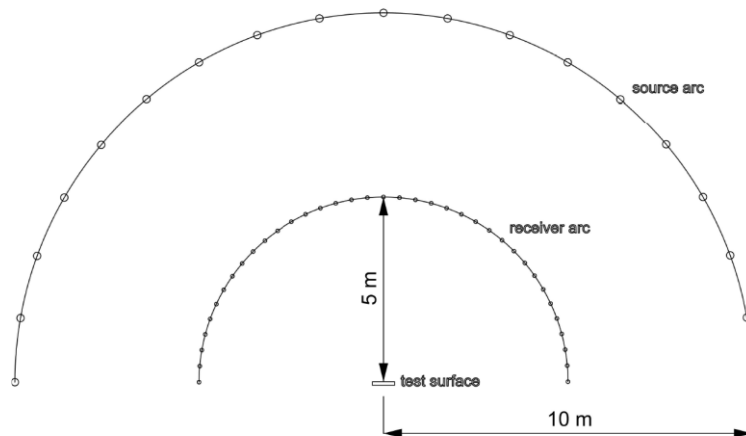


Figure 3: Measurement setup.

3.2 Scattered polar responses

From each impulse response generated by the FDTD numerical simulation, the influence of background reflections is first removed by subtracting the background response from the background response with the test surface, thus removing the direct sound from the impulse response. A Hann window is then applied to the impulse response for smoothing the truncation. The determination of the window location and size was done by visual inspection of the impulse response computed for extreme geometries tested in the optimization process. The same window length was applied to all impulse responses, taking the longest reflection paths as the maximal length of the window while ensuring that no reflections from the boundary room surfaces lay in that portion of the impulse response.

The frequency spectrum of the response is then smoothed by averaging in one-third-octave band to ensure that the standard error is dominated by the general envelope rather than local fluctuations. The mean diffusion is obtained by averaging the standard error for all frequencies, source locations and receiver arcs. The average of all standard errors for all frequencies, source positions, and receiver arcs, is calculated to result in a single-valued broadband diffusion parameter characterizing the uniformity of the scattering from the diffusing surface⁸. This single-valued diffusion parameter ϵ' for m frequencies, incident angles, and receiver arcs, each having a standard error $\epsilon_j(r_s, r, f)$ is⁸

$$\varepsilon' = \bar{\varepsilon} + \frac{2}{\sqrt{m(m-1)}} \sqrt{\sum_{j=1}^m [\omega_j(r_s, r, f) \varepsilon_j(r_s, r, f) - \bar{\varepsilon}]^2}$$

where $\bar{\varepsilon} = \frac{1}{m} \sum_{j=1}^m \omega_j(r_s, r, f) \varepsilon_j(r_s, r, f)$, and $\omega_j(r_s, r, f)$ are weighting functions that can be used to assign relative importance to certain source positions, frequencies, or receiver arcs. In this paper, all weighting functions have been set to 1. The standard error $\varepsilon(r_s, r, f)$ is defined by

$$\varepsilon(r_s, r, f) = 2 \sqrt{\frac{\sum_{\theta=-90}^{90} [L_p(r, \theta) - \bar{L}_p(r, \theta)]^2}{n(n-1)}}$$

with $\bar{L}_p(r, \theta) = \log[\frac{1}{n} \sum_{\theta=-90}^{90} 10^{L_p(r, \theta)}]$, n and the number of samples in 180°.

Semi-circular polar responses are obtained for visualizing the sound pressure level recorded at the 37 receiver positions. An example of polar responses is shown in Figure 4 for a source incidence angle of 30° for 4 different geometries including a flat panel (worst case scenario) and three geometries having the same pattern but different depths. The single value indicated in the polar responses is the standard error of each geometry computed for a source incidence angle of 30° at each 1/3 octave band (only showing up to the 1250 Hz center frequency).

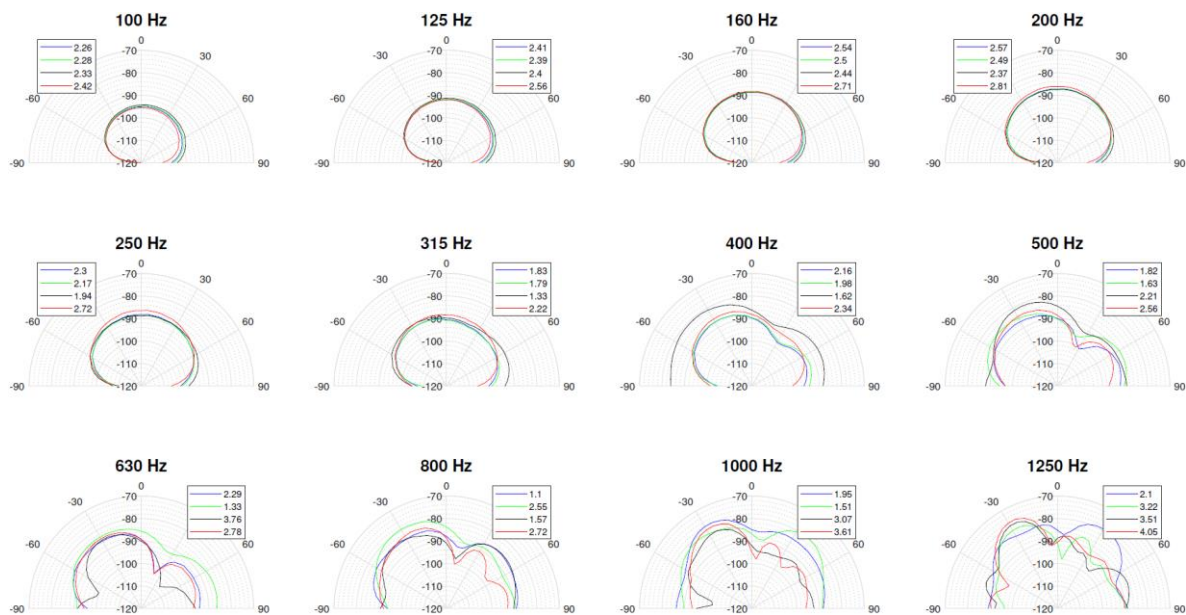


Figure 4: Polar responses extracted from the FDTD simulations of three geometry candidates, having the same pattern but a depth of 5 cm, 10 cm, and 15 cm, respectively (colored in blue, green, and black, respectively), and the flat panel (colored in red) for an incidence source angle of 30°.

4 OPTIMIZATION ALGORITHM

Although the use of a few GPUs allowed to accelerate the FDTD numerical simulations computational time, the evaluation of a single geometry was still relatively computationally costly (approximately 19 hours per geometry for computing all 703 impulse responses), an optimization algorithm is used to explore the parametric space composed of 96 candidates. In addition, the objective function underlying from the numerical simulations is a black-box function. Therefore, a Bayesian approach as implemented in⁹ is employed for this search, because it is well suited for unknown objective functions that are computationally expensive to evaluate. The objective function of the optimization

algorithm is given by the numerical simulations, and the single-valued broadband diffusion parameter defined in the previous section represents its fitness value that has to be minimized by the optimization algorithm. Although the varying geometrical parameters for each geometry are multiple (width and depth of the bars), each geometry candidate is described as an integer in the optimization process (1D process).

Bayesian optimization typically works by assuming that the unknown function is sampled from a Gaussian process and maintains a posterior distribution for this function as observations are made⁹. Except from the prior process that expresses assumptions about the function being optimized, an acquisition function that aims at determining the next point to evaluate must be chosen in the Bayesian approach. The acquisition function is, as opposed to the objective function, an inexpensive function that can be evaluated at a given point that is commensurate with how advantageous evaluating the objective function at this given point is expected to be for the minimization problem. In this paper, the expected improvement acquisition function, that evaluates the expected amount of improvement in the objective function while ignoring values that cause an increase in the objective function, is chosen. Additionally, the first four evaluation points were chosen randomly to initialize the optimization algorithm and no prior knowledge of the objective function was provided to the algorithm. The optimization process was stopped after reaching a number of iterations that was set to 25, 50, 75, and 100 successively for performance testing purposes.

Although the Bayesian approach is used for global optimization problems, one downside of such optimization process is that it does not necessarily give very accurate results. In this paper, two metrics are chosen to assess the efficiency of the optimization algorithm, that are the best estimated value after observing the maximum number of function evaluations and how quickly the estimated objective function evaluation improves under a given number of iterations to execute, also called the area under curve (AUC)¹⁰.

5 RESULTS

In an attempt to validate the optimization algorithm that was used, all of the 96 candidate geometries were first computed and analyzed to provide a better understanding of the results. From this analysis, it resulted that at low frequencies (from 200 Hz to 400 Hz), the deeper the bars are, the smaller the single-valued broadband diffusion parameter is and that below 200 Hz, the diffusion parameter is similar for all depths. At higher frequencies (from 500 Hz to 1250 Hz), the depths of 5 and 10 cm are, however, more effective than 15 cm. At extreme grazing angles (for $\pm 80^\circ$ and below/above incidence source angles), at frequencies from 500 Hz to 1250 Hz, good directional uniformity of the scattering is hard to obtain no matter the depth of the diffuser. These observations are also in line with previous results concluding that optimal diffusion at discrete frequencies is not the same as optimal diffusion across a wide bandwidth¹¹. As an illustration of the result obtained after such optimization process in terms of the directional uniformity of the scattering, the polar response per each 1/3 octave of the output given by the optimization process (i.e. the best of all 96 geometries), as well as for the flat panel and the worst computed geometry, for comparison, are shown in Figure 5 for a source incidence angle of 0° .

As in realistic situations it is likely that a diffuser is expected to be effective for centered source incidence angles rather than for grazing angles such as $\pm 70^\circ$, $\pm 80^\circ$, and $\pm 90^\circ$, the directional uniformity of the scattering created by the diffusers was also investigated for source incidence angles solely ranging from -60° to 60° . As can be seen in Figure 6, the distribution of the diffusion parameter per 1/3 octave band and per depth has the same general form for both source incidence angles combinations. However, it can also be observed that when averaging the diffusion parameter across fewer and more centered source positions than across the whole source semicircle, the gap between the diffusion parameter values for the 3 depths slightly increases for some of the 1/3 octave bands. As an example, while for an average across all sources, the medians for geometries with a depth of 10 cm and 15 cm are 1.94 and 1.97 at 400 Hz, respectively, for an average across the centered sources the medians are 2.04 and 1.73 at the same center frequency. From this observation, it might

be worth considering optimizing a diffuser geometry for only these centered source incidence angles (e.g., from -60° to 60°), as it is likely to represent more realistic cases than if the sources were located on both sides of the diffuser.

Because a random selection of the first four candidates to start the optimization process is made in the Bayesian approach employed in this paper, the required number of function evaluations (i.e. number of iterations) to achieve the best possible point in the observed and estimated objective function evaluations is first investigated. For that aim, the optimization algorithm is set to 25, 50, 75 and 100 iterations, and each run is repeated 20 times. The results show that for a number of 75 and 100 iterations (and likely for another number of iterations laying in these bounds), the observed and estimated objective function evaluations are sufficiently close to each other (means are the same) to consider the optimization algorithm useful in the search (i.e. the number of iterations is less than the number of geometry candidates). An example of a single optimization result search is shown in Figure 7, and boxplots showing all 20 optimization result search for each number of iterations are visible in Figure 7. As can be seen in Figure 7, good convergence between the best observed and estimated objective function evaluations is achieved for 75 and 100 iterations.

Finally, although the optimization algorithm was tested with precomputed objective function evaluations in this paper, as can be seen in Figure 8, the optimization algorithm finds the objective function minimum in an average of 62 iterations, which means that the computational time saved by using the Bayesian approach is of $(96 \text{ candidates} - 62 \text{ iterations}) \times 19 \text{ hour/geometry} = 646 \text{ hours} \approx 9 \text{ days}$, which represents $9/25 = 36\%$ of the total number of days required to compute all geometries.

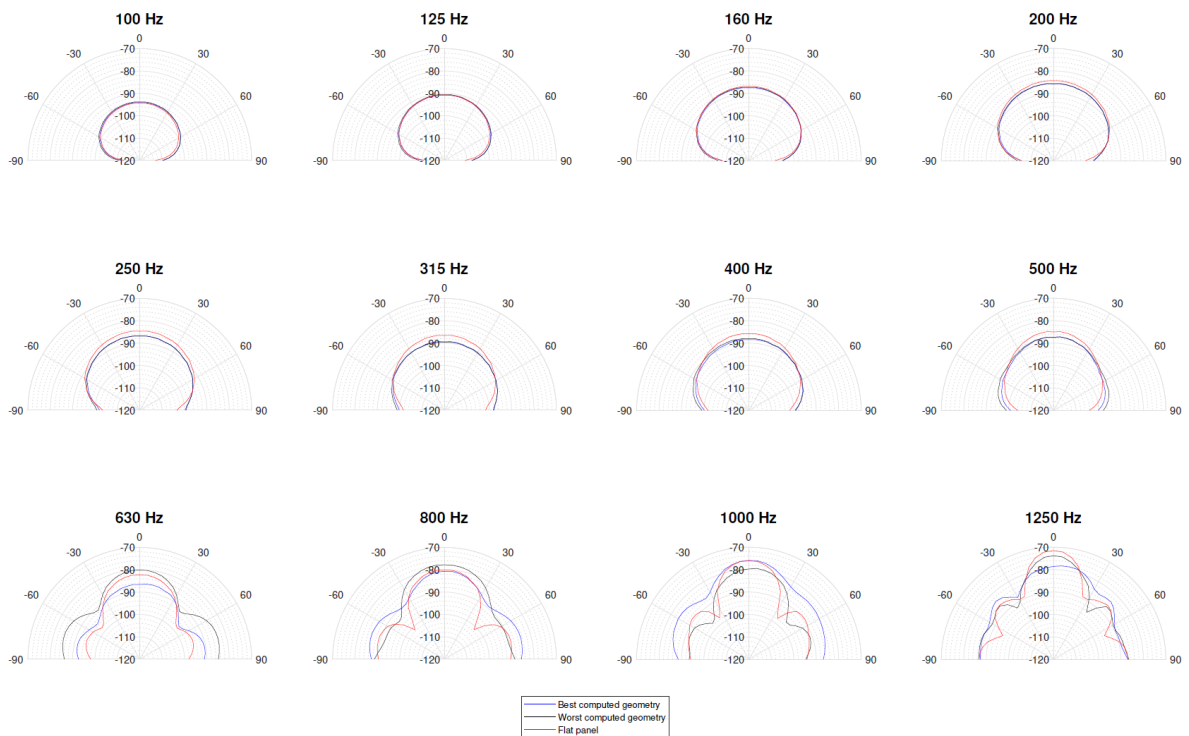


Figure 5: Polar responses of 2 geometry candidates of the optimization process and the flat panel for a source incidence angle of 0° .

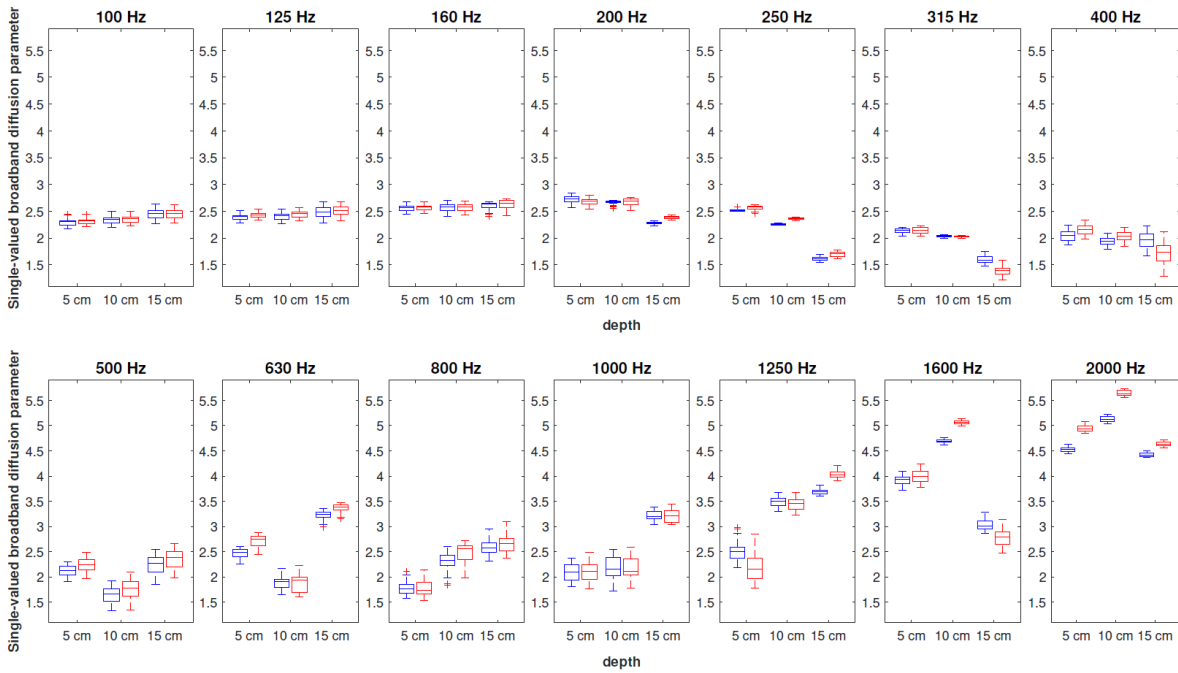


Figure 6: Averaged single-valued broadband diffusion parameter across all 19 sources (colored in blue) and across sources from -60° to 60° (colored in red) per 1/3 octave band. The smaller the diffusion parameter the better.

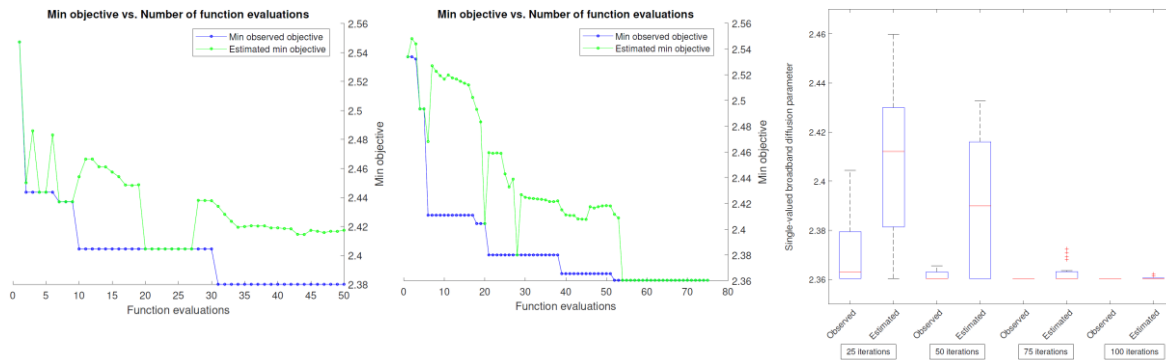


Figure 7: Best observed and estimated objective function evaluations for 50 (top left) and 75 (top right) iterations, and as a function of number of iterations (bottom).

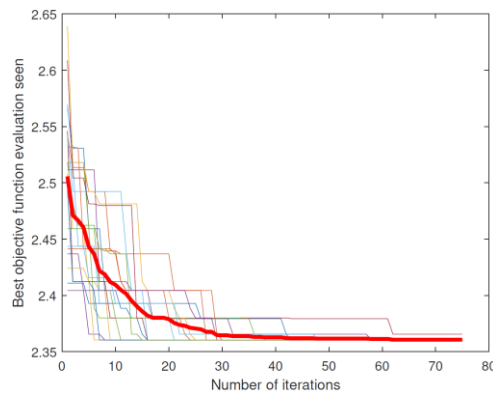


Figure 8: Twenty repetitions of the best seen objective function evaluation (the thick red line is the average) as a function of number of iterations.

6 CONCLUSIONS AND FUTURE WORK

Parametric modeling tools (Rhinoceros software and Grasshopper plugin), FDTD numerical simulations, and an optimization algorithm using the Bayesian approach have been used to automatically generate 96 different diffuser geometries, evaluate the single-valued broadband diffusion parameter for each of these geometries, and optimize the process of searching for the best of these candidates, respectively. The framework presented could be used to study any other geometry and geometrical parameters since it uses parametric tools to generate automatically the geometries. It is shown that with 75 iterations, using the optimization algorithm accelerates the process since the best estimated objective function converges towards the best observed objective function within less iteration number than the total of geometry candidates.

Although the numerical dispersion inherent to FDTD simulations has been somehow controlled by oversampling the sampling frequency of the domain by a factor of 10 to result in an approximate phase velocity error of 2%, further work should focus on quantifying more precisely the error contained in the present simulation results. Indeed, since the dispersion error is also distance and propagation direction dependent, and the diffusion coefficient measurement setup applied in this paper requires long propagation distances and several propagation directions depending on the receiver position, it is likely that the error is non negligible, and also not uniform across all receivers.

In order to determine if the main focus of such an optimization process should be made on the time taken by the optimization algorithm rather than on the quality of its result (e.g. local minimum vs. global minimum), the perceptual effect of such diffusing surfaces should be investigated. Indeed, if there exists any perceivable differences between optimized and non-optimized diffuser geometries, it becomes relevant to compute more iterations in the optimization algorithm to ensure that the parametric space's global minimum rather than one of its local minimums can be found.

Acknowledgments: The authors wish to thank Jukka Saarelma for providing the FDTD solver for room acoustics. This project has received funding from the European Union's Horizon 2020 research and innovation programme under grant agreement No 721536.

7 REFERENCES

1. Cox, T. J. The optimization of profiled diffusers. *The J. Acoust. Soc. Am.* 97, 2928–2936 (1995).
2. Patraquim, R., Godinho, L. & Amado Mendes, P. Design and optimization of the sound diffusers using radial basis functions-based shapes and genetic algorithms. *The J. Acoust. Soc. Am.* 141, 3664–3664 (2017).
3. Cox, T. & d'Antonio, P. *Acoustic absorbers and diffusers: theory, design and application* (Crc Press, 2016).
4. Cox, T. & d'Antonio, P. AES information document for room acoustics and sound reinforcement systems-characterization and measurement of surface scattering uniformity. *J.Audio.Eng.Soc.* (2001).
5. ISO 17497-2:2012. Acoustics - sound-scattering properties of surfaces - part 2: Measurement of the directional diffusion coefficient in a free field (2012).
6. Saarelma, J. Finite-difference time-domain solver for room acoustics using graphics processing units. *Master's thesis, Aalto Univ. Finland* (2013).
7. Saarelma, J., Botts, J., Hamilton, B. & Savioja, L. Audibility of dispersion error in room acoustic finite-difference time-domain simulation as a function of simulation distance. *The J. Acoust. Soc. Am.* 139, 1822–1832 (2016).
8. Cox, T. J. Designing curved diffusers for performance spaces. *J. Audio Eng. Soc.* 44, 354–364 (1996).
9. Snoek, J., Larochelle, H. & Adams, R. P. Practical bayesian optimization of machine learning algorithms. In *Advances in neural information processing systems*, 2951–2959 (2012).
10. Dewancker, I. et al. A stratified analysis of bayesian optimization methods. *arXiv preprint arXiv:1603.09441* (2016).
11. Cox, T. Acoustic diffusers: the good, the bad and the ugly. *Proc. Inst. Acoust.* (2004).